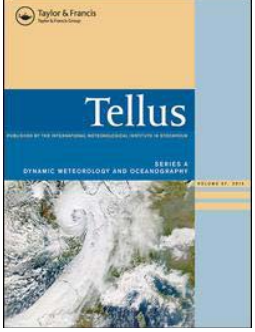

Tellus A: Dynamic Meteorology and Oceanography

ISSN: (Print) 1600-0870 (Online) Journal homepage: https://www.tandfonline.com/loi/zela20

Off-bottom turbulence expansions of unbounded flow over a deep-ocean ridge

Hans van Haren

To cite this article: Hans van Haren (2019) Off-bottom turbulence expansions of unbounded flow over a deep-ocean ridge, Tellus A: Dynamic Meteorology and Oceanography, 71:1, 1-10

To link to this article: https://doi.org/10.1080/16000870.2019.1653137

Tellus SERIES A DYANAMIC METEOROLOGY AND OCEANOGRAPHY
PUBLISHED BY THE INTERNATIONAL METEOROLOGICAL INSTITUTE IN STOCKHOLM

Off-bottom turbulence expansions of unbounded flow over a deep-ocean ridge

By HANS VAN HAREN*, *Royal Netherlands Institute for Sea Research (NIOZ) and Utrecht University, Den Burg, the Netherlands*

(Manuscript received 21 September 2018; in final form 1 August 2019)

ABSTRACT

Internal wave breaking upon sloping seafloors is a potential source of turbulent mixing in the deep-ocean, but we lack details on off-bottom breaking. Turbulence processes are relevant for the dispersal away from the seafloor of suspended materials like those emanating from thermal vents and artificial mining activities. For the present study, high-resolution temperature sensors have been moored up to 406 m above a slope of a 2000 m deep crest of the Mid-Atlantic Ridge. In addition to familiar observations of on-slope propagating highly nonlinear bores dominating turbulent mixing near and in contact with a sloping seafloor, the present observations show occasionally larger than 100 m tall turbulence expansions between 100 and 250 m above the seafloor at the transition from on- to off-slope flow. The details of such turbulence expansion are reminiscent of an asymmetric quasi-mode-2 internal hydraulic jump, with some specific differences compared with near-surface hydraulic jumps. As the expansion is generated at the transition from weak to steep edge of a saw-tooth internal tidal wave, it leads turbulence and stratification in two directions: One down to the seafloor in the direction of tidal phase propagation; the other more horizontally and slightly upward associated with near-homogeneous overturning remaining well away from the seafloor while preceding and sharpening near-bottom frontal bores. The mean turbulence dissipation rates O(10^{-8}–10^{-7} m^2s^{-3}) associated with these expansions are half an order of magnitude less than those of on-slope propagating near-bottom bores, while about equal in duration. As for bores, their appearance, intensity and timing vary every tidal cycle.

Keywords: geophysical and geological flows; internal waves; stratified turbulence; hydraulic jumps; ocean observations

1. Introduction

Studies on turbulence processes are important for the understanding and modelling of the redistribution of nutrients and matter in the ocean via diapycnal fluxes. Near-bottom turbulence processes may bring materials from the seafloor in resuspension. Ocean-interior turbulence processes and flows may disperse the resuspended materials. Major contributors to such turbulence are internal waves breaking over sloping underwater topography (e.g. Eriksen, 1982; Thorpe, 1987). Detailed observations of internal wave-induced turbulence have demonstrated particularly strong diapycnal mixing during short bursts of the passage of nonlinear waves and bores above deep-ocean sloping topography (Bogucki et al., 1997; Grue et al., 2000; Klymak and Moum, 2003; Hosegood et al., 2004). The on- (or up-)slope propagating bores of breaking internal waves occur just after the transition from off- (or down-)slope flow to on-slope near-bottom flow of the large-scale 'carrier' wave, the dominant internal motion. This dominant internal motion interacting with seafloor topography can be a propagating semidiurnal internal tide (e.g. Dauxois et al., 2004; van Haren and Gostiaux, 2012; Winters, 2015), but also a sub-inertial mesoscale motion (Hosegood et al., 2004) and a trapped ('not freely propagating') diurnal internal tide (Cyr et al., 2016). In essence, the carrier wave excites an on-and-off-slope sloshing motion of lesser and more buoyant fluid, which involves rapid alternation within a wave's cycle of mixing and restratification due to straining deformation and advection. The slopes have topographic scales that exceed those of the typically 1-km excursion scale of a carrier wave and do not generate internal hydraulic jumps (e.g. Dale and Inall, 2015).

*Corresponding author. e-mail: hans.van.haren@nioz.nl

Citation: Tellus A: 2019, **71**, 1653137, https://doi.org/10.1080/16000870.2019.1653137

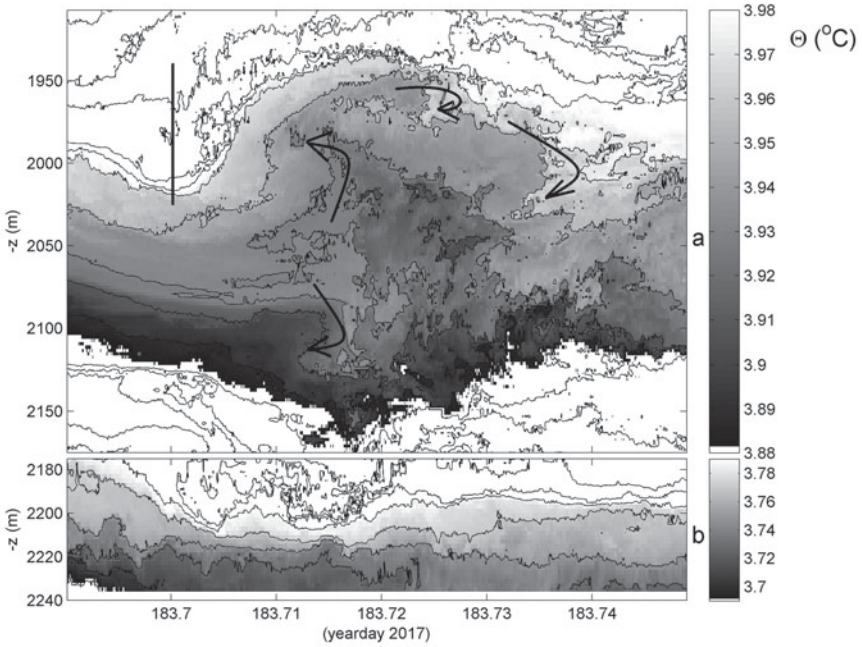

Fig. 1. Example of detailed off-bottom >100-m tall turbulence expansion burst from 1.5 h of high-resolution conservative (~potential) temperature data observed on July 2 (yearday 183) between 8 and 405 m above the bottom 'mab', with 19 flawed T-sensors interpolated. Black contours are drawn every 0.02 °C. (a) Middle 268 m of the T-sensor range. The black vertical bar indicates the transition moment to supercritical flow, the arrows some overturning interpretations. (b) Lower 65 m above the bottom (seafloor = horizontal axis) with different colour ranges.

Within a carrier wave cycle, the on-slope propagating bores are generally the only turbulent overturn generators that actually touch the seafloor rather than pushing isopycnals downward to within a few meters above the bottom (hereafter, mab, for short). As such, bore turbulence is important for the resuspension of sediments and associated nutrients (Hosegood et al., 2004). At sites more than a few 100 m below seamount-summits or shelf-breaks bores are found most intense above steep seafloor slopes that are, e.g. supercritical for the semidiurnal internal tide (van Haren et al., 2015; Winters, 2015; Sarkar and Scotti, 2017).

Numerical modelling of flow over seamounts also demonstrated large turbulent activity over topographic crests with steep, i.e. semidiurnal-internal-tide-supercritical, slopes (Legg and Klymak, 2008). However, in contrast with the above on-slope propagating bores this intense turbulence activity over a crest was associated with off-slope flow. It was generated after the transition from on- to off-slope tidal flow and characterized as a hydraulic jump at some distance, typically 100 m, below the seamount summit and extending about 250 m vertically. By its off-slope advection, it was observed to push isopycnals downward towards the seafloor and create larger than 100 m tall nearly homogeneous layering (e.g. Musgrave et al., 2016; Thorpe et al., 2018). The shape of the hydraulic transition was characterized as 'oval' and 'mode-2' by a model of Thorpe et al. (2018), more or less fitting limited profiling observations in a deep-ocean through-flow.

In this paper, moored high-resolution temperature T-observations are analysed on rather rare intense off-bottom turbulence upon the turn of the semidiurnal tide from on- to off-slope flow in the interior about 200 m above the seafloor (Fig. 1). The turbulence expansion occurs in the tidal phase 1 to 2 h before 'pre-frontal bore mixing', the recently reported large near-homogenization that pushes a stratification anomaly to very near the seafloor just before frontal bores propagate on-slope (van Haren et al. 2017). While the here reported process of turbulence expansion is reminiscent of an internal hydraulic jump, the previously reported process of pre-frontal mixing is not associated with an internal hydraulic jump. It is hypothesized that both processes are driven by internal tide topography interactions of significantly different scales. It will be demonstrated that the expansion determines the conditions for both the following large pre-frontal interior overturning and the subsequent associated near-bottom highly nonlinear frontal bore.

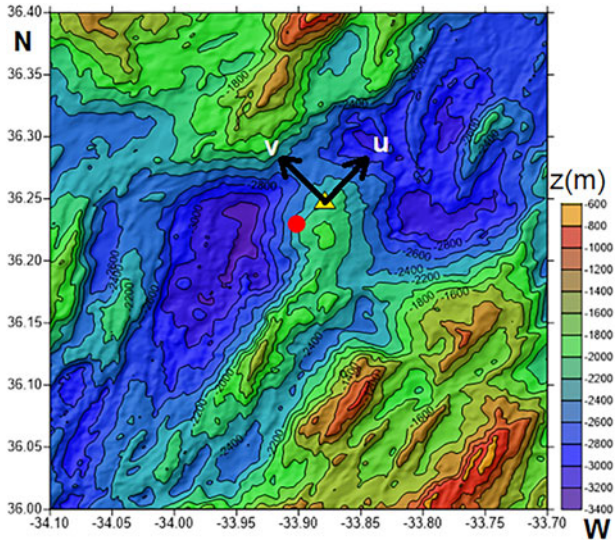

Fig. 2. Bathymetric map part of the Mid-Atlantic Ridge, southwest of the Azores (P). The site of the mooring is indicated by the yellow triangle centring the positive directions of the local along- and cross-slope current components on the north-slope of Rainbow crest. The red dot indicates Rainbow's main hydrothermal vent. Multibeam data, 100×100 m grid.

2. Materials and methods

Observations were made using a single mooring that was deployed from 28 June (yearday 179) to 10 July (yearday 191) 2016 at 36° 14.86N, 33° 52.61W, 2240 m water-depth, on the northwestern slope of Rainbow Ridge (Fig. 2). The mooring site was about 3 km NE from and 150 m shallower than the Rainbow hydrothermal vents, which are not traceable in temperature at distances more than 1 km away horizontally (German et al., 1996; Khripounoff et al., 2001; Thurnherr and Richards, 2001). Strong turbulence processes with estimated diffusivities of up to 4×10^{-2} m^2 s^{-1} (Walter et al., 2010) mix vent waters with that of surrounding water masses. The anchor weight was positioned about 100 m below the local crest. The local bottom-slope is $\beta \approx 0.22 = 13°$. Semidiurnal lunar M_2 tidal motions dominate currents, having near-bottom polarized ellipses with cross-slope amplitude of $v = 0.15$ m s^{-1} and along-slope amplitude of $u = 0.10$ m s^{-1}, and near-circular polarization of u, $v = 0.10$ m s^{-1} at 150 mab (van Haren et al., 2017).

The mooring consisted of a 710 m long nylon-coated 5 mm diameter steel cable extended vertically between a single heavy top-buoy and a 550-kg anchor weight. The net buoyancy of the mooring was 250 kg and the net anchor weighed 200 kg. Tilt- and pressure sensors indicated that top-buoy motions were less than 0.1 m vertically and less than 8 m horizontally under total current speeds of up to 0.3 m s^{-1}. A low-resolution downward 'looking' 75 kHz Teledyne/RDI Acoustic Doppler Current Profiler ADCP was mounted in the top-buoy and a single-point Nortek AquaDopp current meter was at 7 mab. The ADCP sampled 120 vertical bins of 5 m each at a rate of once per 60 s. The 20° slanted beams of the ADCP caused an averaging over several 100's of meters horizontally, so that its current measurements only resolved the large spatial scales. The single-point current meter also sampled the 3D velocity components [*u, v, w*], w denoting the vertical component, but from a volume of about 0.5 m^3 at a rate of once per 10 s.

To the lower 398 m of the mooring cable 200 'NIOZ4' self-contained high-resolution T-sensors were taped every 2 m. The lowest sensor was at 8 mab. The sensors sampled at a rate of 1 Hz, with a precision better than 5×10^{-4}°C and a noise level of less than 1×10^{-4}°C (van Haren, 2018). Every 4 h all T-sensors were synchronized to a standard clock, so that the 398 m nearly true vertical profile was measured in less than 0.02 s, every second. Nineteen sensors showed calibration or electronic problems and their data were linearly interpolated. After correction for slight compressibility and drift effects of about 1 mK/mo, the T-data were converted into 'Conservative' (~potential) Temperature data Θ (IOC, SCOR and IAPSO, 2010). They were used as a tracer for density anomaly σ_2-variations referenced to 2000 dbar following $\delta\sigma_2 = \alpha\delta\Theta$, where $\alpha = -0.075 \pm 0.001$ kg m^{-3}°C^{-1} denotes the apparent local linear relationship-coefficient. With this relation, the standard deviation in density anomaly estimates from temperature is about 8×10^{-4} kg m^{-3}. The tight relation was established from the lower 500 m of a shipborne conductivity–temperature-depth

(CTD) profile obtained within 1 km from the mooring site. In the dataset under investigation, salinity intrusions disturbing this relationship did not occur.

The number of T-sensors and their spacing of 2 m, in combination with their low noise level and the tight density–temperature relationship, allowed for the quantification of turbulence by estimating turbulence dissipation rate ε and vertical eddy diffusivity K_z via the reordering of unstable overturns making every 1-Hz sampled density-(temperature-)profile a statically stable one (Thorpe, 1977). For details of the method for moored T-sensor data and the use of the standard oceanographic parameterizations therein the reader is referred to van Haren and Gostiaux (2012). The standard parameterizations involved an Ozmidov/Thorpe overturning scale ratio of 0.8 and a mixing efficiency of 0.2. These values were established from ocean, not laboratory, observations after sufficient averaging (e.g. Dillon, 1982; Oakey, 1982). Although the precise reason is still unknown, Gregg et al. (2018) suggest that the relatively efficient ocean mixing may be because the ocean is a high Reynolds number environment having values between 0.1 and 10 million that are much higher than achievable in numerical or laboratory modelling. Ocean turbulence is also a mix of free convective and shear-induced motions (Cimatoribus and van Haren, 2015). In particular above sloping topography, relatively high mixing efficiencies are provided where rapid restratification follows internal wave breaking due to the sloshing back-and-forth of the carrier wave in addition to along-isopycnal dispersal of mixed waters into the interior (Slinn and Riley, 1996; Winters, 2015). The 1-Hz sampling rate and 398 m vertical range of the moored T-sensors ensure sufficient averaging for reliable statistics of turbulence parameter estimates. In the following, averaging over time is denoted by $[\ldots]$, averaging over depth-range by $<\ldots>$. Mean eddy diffusivity values are obtained by averaging the flux first.

3. Observations and results

Smooth low-mode isotherm displacements are observed to suddenly expand in a local mode-2 structure of opposing isotherms 100 m tall and rather turbulent as evidenced from more irregular isotherms after day 183.7 (Fig. 1). The upper isotherms (around $z = -2000$ m, day 183.7) steeply rebound upward while the lower isotherms continue descent (between $-2050 < z < -2100$ m). This happens when the flow becomes supercritical, following Thorpe et al. (2018), here at day 183.70. The shape of the transition to turbulence expansion between days 183.71 and 183.72 resembles a mushroom or perhaps a medusa, on its side, but not an oval as in Thorpe et al. (2018). Its more or less vertical front around day 183.71 seems to consist of a vortex pair (see arrows in Fig. 1a). As these vortices do not occur at exactly the same time they give an asymmetric appearance to the entire expansion. While the larger than 100 m tall interior overturn does not reach the seafloor, the irregular isotherms move downward at day 183.72, which strains the layer in the lower 30 mab. Although the expansion occurs every M_2-tidal period, its form and its timing, but less so to within error its intensity (see below), vary between different tidal periods. Its turbulent core is always observed at about 200 mab. As the lower range of turbulence is at about 100–150 mab, the near-buoyancy frequency wave collapse into expansion is likely triggered by the internal tidal flow over the local crest.

3.1. One-day variability

The environmental and temporal setting in which the off-bottom internal turbulence expansion occurs is as follows (Fig. 3). The about 150 m tall M_2-tidal isothermal (black contour) displacements are not sinusoidal but close to a saw-tooth form in the z–t plane. The isotherms are most vertical at the transition between interior off-slope (warming phase) and on-slope (cooling phase) flow, or just thereafter during on-slope near-bottom flow. The phase in the tide with most vertical isotherms, i.e. weakest density stratification, is associated with pre-frontal mixing described in van Haren et al. (2017), occurring around day 183.8 and day 184.3 in Fig. 3, and with near-bottom frontal bore motions (e.g. Hosegood et al., 2004), around day 183.85 and day 184.35 in Fig. 3. In contrast, strongest large-scale (∼100 m vertical scale length) density stratification occurs some distance off the bottom around $z = -1950$ m during the off-slope phase of near-bottom flow around day 183.5 and day 184.0. The density stratification carries near-buoyancy (high-) frequency internal waves, as seen in the wave pattern of isotherms and, more clearly and throughout the image, in the vertical current alternating sign in time while being uniform over 100's of meters of vertical range (Fig. 3a). The high-frequency internal waves oscillating at their natural restoring force 'buoyancy' frequency N may be generated, e.g. by nonlinear motions like bores (their trailing waves) or by inertial/tidal shear. The horizontal current components organize in sloping bands of alternating sign (direction) in the z,t-plane (Fig. 3b). During the down-going warming phase of the tide, between days 183.5 and 183.7 and between days 183.9 and 184.15, the bands have approximately the same gentle slope as the stratification (Fig. 3b, example for v, similar for u (not shown). The phase propagation is downward like that of the crests of the isotherms, as is expected for internal tidal energy propagating upward after generation (or reflection) at the

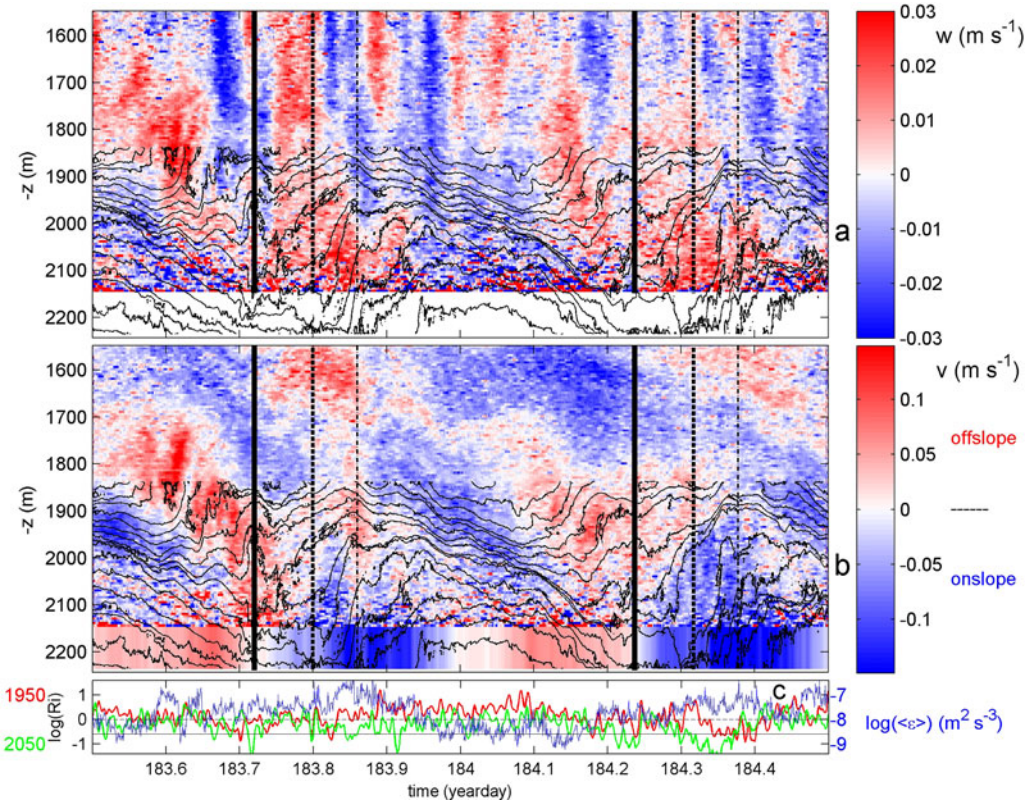

Fig. 3. One day of data around Fig. 1 of high-resolution 398-m range T-observations superposed on low-resolution 600-m range ADCP observations. (a) Vertical current component, smoothed over 600 s intervals. Black contours indicate Θ every 0.05 °C. The seafloor is at the horizontal axis. The black-solid vertical bars indicate approximate times of internal turbulence expansion, the thick dashed lines those of pre-frontal mixing (van Haren et al., 2017) and the dash-dotted lines those of near-bottom frontal bore. Each set of lines is shifted an exact multiple of the semidiurnal lunar tidal period. (b) Cross-slope current component with the lower 95-m thick bar coloured by the current meter data at 7 mab (up to the lowest bin of good ADCP-data at 100 mab). Black contours are copied from a. for reference. (c) Logarithm of gradient Richardson number for hourly smoothed 100-m-averaged values around $z = -1950$ m (red) and $z = -2050$ m (green), with horizontal black lines indicating (in)stability transition values of 0.25 (solid; Miles and Howard, 1964) and 1.0 (dashed; Abarbanel et al., 1984). Additionally, the logarithm is given of the record of vertically 8–405 mab-mean dissipation rate (in blue, scale to right).

seafloor. The banding in the *z,t*-plane of *v*-component data appears interrupted, with enhanced/decreased current values having extents of about 150 m in the vertical and the buoyancy scale of nearly 2 h in time. This 'intermittent' or patchy character has also been observed in internal tidal 'beams' near their source off the continental slope in the Bay of Biscay (van Haren et al., 2010) where some of the world's prominent internal tides are generated (Pingree and New, 1991).

Every M_2-tidal cycle, the sloping pattern in the *v*-component is interrupted by a near-vertical 200 m tall band of positive (off-slope) current, in Fig. 3b between about $-1850 < z < -2100$ m around day 183.7 and day 184.2. This is when the off-bottom turbulent internal expansion occurs in the shape of local quasi mode-2, although being different in overturning-details around day 184.2 compared with that of Fig. 1. Averaged over the about 200-m tall and 1.5-h duration, i.e. about 75% of one buoyancy period, lasting expansion, the turbulence intensity varies by about a factor of 1.5 between the tidal periods: A non-significant difference between mean values of $<[\varepsilon]> = 4 \pm 3 \times 10^{-8}$ m^2 s^{-3} and $<[K_z]> = 1.1 \pm 0.5 \times 10^{-2}$ m^2 s^{-1}, while $<[N]> = 8 \pm 2 \times 10^{-4}$ s^{-1}.

After the turbulent overturn expansion within about 3.5 h, the upper set of isotherms goes up to the depth level of their maximum height above the bottom, the tidal isotherm-crest, whilst the lower isotherms eventually reach (close to) the seafloor, before becoming near-vertical. While the then following on-slope propagating near-bottom frontal bore carries the peak in turbulence values per M_2-tidal period (only 398-m-vertically averaged values are given in Fig. 3c) around days 183.85 and 184.35, the turbulence associated with the off-bottom expansion is not small. It is about half an order of magnitude

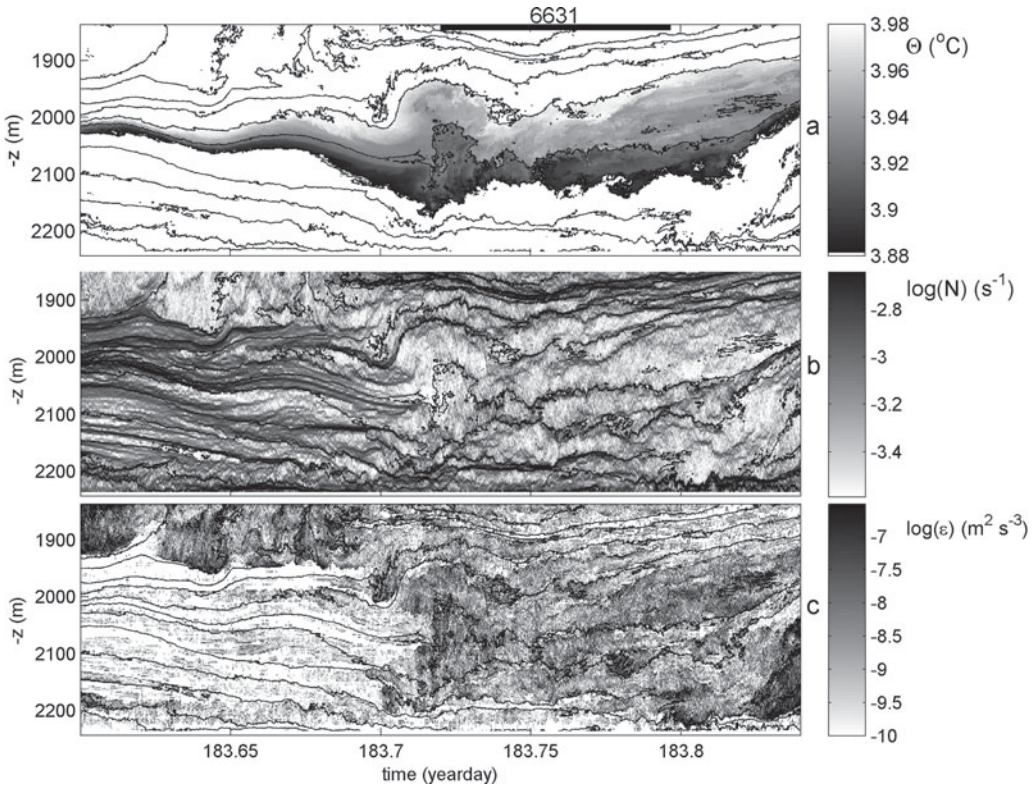

Fig. 4. Six hours of data around Fig. 1 from high-resolution T-sensor data. (a) Conservative Temperature. Black contours are drawn every 0.05 °C. The horizontal bar indicates the mean buoyancy period (in s) for the entire panel. The seafloor is at the horizontal axis. (b) Logarithm of buoyancy frequency from reordered Θ, with black contours copied from a. for reference. (c) Logarithm of un-averaged dissipation rate from data in a. using the method of Thorpe (1977), with black contours copied from a. for reference.

smaller than the near-bottom frontal bore but about one order of magnitude larger than the turbulence generated around the strongest stratification and, presumably, largest shear $\mathbf{S} = [du/dz, dv/dz]$ of the off-slope propagating phase (here near the beginning of the panel, and between days 183.95 and 184.15). The expansion occurs around the time of minimum gradient Richardson number $\mathrm{Ri} = N^2/|S|^2$ (Fig. 3c), which is found below the criterion of linear stability of Ri = 0.25 (Miles and Howard, 1964). Because of the low resolution of the ADCP, Ri is computed over 100 m vertical intervals around $z = -1950$ and $z = -2050$ m. It is noted that generally $\mathrm{Ri} \approx 1$ or marginally stable for nonlinear 3D flows (Abarbanel et al., 1984), except perhaps during the warming downward phase of the M_2-tide.

For the range of observations in Fig. 3, the one-day 398-m-average turbulence values are $<[\varepsilon]> = 4 \pm 3 \times 10^{-8}$ m^2 s^{-3} and $<[K_z]> = 1.3 \pm 0.7 \times 10^{-2}$ m^2 s^{-1}, while $<[N]> = 9 \pm 3 \times 10^{-4}$ s^{-1}. The turbulence is not only variable in time, over three orders of magnitude (*cf.*, the 398-m-averaged values in Fig. 3c), but also in the vertical. A major separator is visible around $z = -1900$ m, where both the w- and the v-(also u-)components change their patterns. It was suggested by van Haren et al. (2017) that this was associated with the flow over the top of Rainbow Ridge, which is found at this depth.

3.2. Turbulence transition detail

Part of the transition around $z = -1900$ m is visible in a 6-h detail (Fig. 4). While the undulating stratification shows only weak turbulence in the lower 300 mab up to day 183.7, turbulent overturning is visible above, which marks the transition from off-slope flow above to on-slope flow below (*cf.*, Fig. 3b). As suddenly on day 183.71 a large part of the 300 mab range switches to off-slope flow, the thin-layer isotherms (Fig. 4a,b) turbulently mix into a 200 m weakly stratified core. The turbulence dissipation rate is now concentrated between $-1950 < z < -2150$ m (Fig. 4c), while the strongest thin-layer stratification is pushed up (around $z = -1900$ m) and down (around $z = -2200$ m).

For this 6-h period, depth-time averages amount $<[\varepsilon]> = 5 \pm 3 \times 10^{-8}$ m^2 s^{-3} and $<[K_z]> = 1.4 \pm 0.7 \times 10^{-2}$ m^2 s^{-1}. These values are non-significantly larger than the above tidal-period mean values. However,

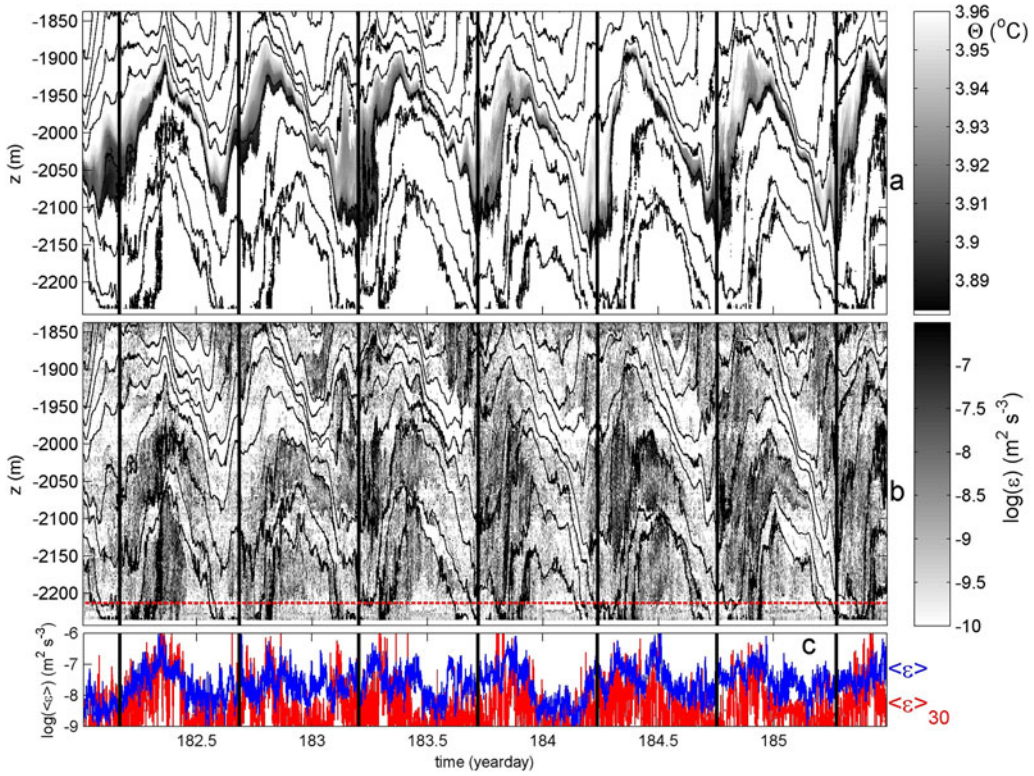

Fig. 5. Three-and-a-half days of data around Fig. 1 demonstrating the straining and off-bottom turbulent bursting varying every tidal period. (a) Conservative temperature. Black contours are drawn every 0.09 °C. The seafloor is at the horizontal axis. The black-solid vertical lines indicate approximate times of internal turbulence expansion. The lines are shifted by an exact multiple of the semidiurnal lunar tidal period. (b) Logarithm of un-averaged dissipation rate from data in a. using the method of Thorpe (1977), with black contours copied from a. for reference. The red horizontal dashed line is at 30 mab. (c) Logarithm of vertically averaged dissipation rate, in blue for the entire temperature sensor range between 8 and 405 mab, in red for near-bottom 8 to 30 mab.

it indicates that also during the warming phase waters can occasionally be quite intensely turbulent, at some distance off the bottom. In general, the observed individual overturns have shorter duration than the shortest possible free internal wave buoyancy period, with duration of large overturning approaching the buoyancy period, like around day 183.8.

3.3. Off-bottom turbulence variability with depth and time

From a 3.5 days image, it is seen that the off-bottom turbulent overturns occur around $z = -2000$ m at the transition from relatively weak to strong turbulence and that they are followed by intensified turbulence in two pathways (Fig. 5): One stays at $z = -2000$ m or is slightly going upward; another slants downward towards the bottom and reaches close to the seafloor, eventually preceding the near-bottom frontal bore. The turbulence internal expansions occur every tidal cycle, but their timing may be 1 h off with respect to the same phase in the semidiurnal lunar tidal period (Fig. 5a) and the 1 h, 270-m average turbulence dissipation rate varies with a diurnal inequality by a factor of two (Table 1), which is within error bounds.

Thus, not only the horizontal current components and isotherms slant in the z,t-plane, but also the extent of turbulent overturning. In general, a tidal period's weakest turbulence is associated with stronger stratification during the off-slope/warming phase. In comparison with the near-bottom (<30 mab) mean turbulence values, the 398-m-averaged values are generally larger, except when a frontal bore moves on-slope (e.g. on days 183.3, 183.83, and 184.37 in Fig. 5c). Or, when interior turbulence activity is thus low that the near-bottom pre-frontal push-down of isotherms generates efficient mixing (e.g. on days 183.1 and 183.8). In all these cases, the turbulence is generated by internal wave breaking, as the background near-bottom turbulence intensity associated with the tidal frictional flow does not generate large $<\underline{\varepsilon}>_{30}$ on days 183.65 and 184.1 when near-bottom tidal currents peak, *cf.* Fig. 3c, for example. This confirms other frictional

Table 1. Turbulence dissipation rates averaged over 1 h and 270 m between $-2175 < z < -1905$ m for seven internal turbulence expansions of Fig. 5. In the table, the observed start-times of the depression immediate before expansion are indicated, which are not necessarily separated by a multiple of the semidiurnal lunar tide (period of 0.5175 day).

Start-time (yearday)	182.17	182.69	183.11	183.70	184.17	184.73	185.22
$[<\varepsilon>]$ ($\times 10^{-8}$ m^2 s^{-3})	1 ± 0.6	6 ± 4	2 ± 1.5	6 ± 4	2 ± 1.5	6 ± 4	2 ± 1.5

'bottom boundary layer' thicknesses, which are typically O(10 m), for given eddy viscosity values (Prandle, 1982; Soulsby, 1983).

4. Discussion and conclusions

The observed time-depth distribution of turbulence parameters lends support to the notion that sloping ocean topography is not a flat boundary over which the Prandtl frictional mixing length concept applies. Instead, other mixing mechanisms like internal wave breaking prevail. It also lends support to the notion that internal wave breaking is a rather efficient means of mixing, as the mixing efficiency of an average 0.2 is relatively high due to the repeated periodic restratification (cf. the isopycnals in the various graphs presented) by the large-scale internal waves sloshing back and forth against the topography. The mixing is expected to be more efficient than shear-induced turbulence in a frictional near-homogeneous bottom boundary layer, and less efficient than natural free convection (e.g. Dalziel et al., 2008). Here, tidal flows have an excursion length of typically 1 km, flowing over the ridge-crest. The M_2-internal tide may be generated locally over the ridge-crest, and may also propagate from numerous other sources across the Mid-Atlantic Ridge. The single mooring cannot distinguish the origin of the internal waves.

The shape of the local mode-2 turbulence expansion at about 200 m above the seafloor is mushroom- or medusa-like, but not oval as suggested by Thorpe et al. (2018). The expansion thus resembles a horizontal dipolar vortex. Small vortices asymmetrically distributed above and below may be the cause of the slightly forward tilt of the entire expansion with the upper overturn passing the T-sensor array earlier than the lower overturn. This is also observable in the oval shape in Thorpe et al. (2018), but more explicit in the present details.

It was suggested by van Haren et al. (2017) that the turbulence associated with pre-frontal mixing is not a result from hydraulic control of the tidal flow over the ridge. This was because $\beta N \approx 1.5\sigma_{M2}$, <2–$3\sigma_{M2}$ or not enough time for the vertical signal to propagate before the tide reversal, e.g. (Inall et al., 2005). However, hydraulic flow control is important for the turbulent internal expansion 2 h earlier in the M_2-tidal phase. This is because stratification is concentrated in thin layers due to straining and varies between large-100-m-scale mean buoyancy frequency N, used in the above equation, and maximum small-2-m-scale $N_m \approx 6$ N here. The downward sloping local large-100-m-scale stratification N_l gives $\beta N_l \approx 2\sigma_{M2}$. The isopycnals are then either squeezed by tidal shear and/or by high-frequency internal waves, commensurate the 5000 s short-scale buoyancy period, which shortens further to 3000 s before turbulence expansion.

It is noted that off-bottom turbulence expansions are observed in an area where the large $>$ 1 km scale bottom-slope is significantly steeper than internal M_2-tidal wave slopes (van Haren et al., 2017), so that critical wave reflection does not seem a dominant mechanism in generating them. It is also noted that off-bottom turbulence expansions vary in overturning details and timing while showing roughly the same averaged turbulence values every tidal period, similar to the twice more turbulent near-bottom frontal bores. The appearance of internal expansions is that of an asymmetric internal hydraulic jump, possibly propagating lee wave (Mohri et al., 2010), with its turbulence not directly affecting the seafloor and, thus, little affecting the resuspension of sediment, in contrast with near-bottom frontal bores. However, once sediment has been whirled-up by a near-bottom bore and is kept in suspension for half a tidal period, it is hypothesized that the internal expansion may contribute to further dispersal into the interior.

To conclude: Above the slopes of local ridge-crests the bursting of turbulence is thus observed in three stages each separated by 1 to 2 h: Interior off-bottom expansion as an internal hydraulic jump at the transition from on- to off-slope tidal flow phase (this paper), leading to: Pre-frontal near-homogeneous waters not associated with an hydraulic jump but which intensify the stratification that is pushed towards the bottom (van Haren et al., 2017), and: Which near-vertically extends upward upon the passage of a near-bottom upslope propagating frontal bore (e.g. Klymak and Moum, 2003; Hosegood et al., 2004). The sequence takes up half a period of a large-scale carrier wave, such as an internal tide.

In comparison with near-surface internal hydraulic jump observations (e.g., Armi and Farmer, 2002; Cummins et al., 2006), the deep off-bottom turbulence expansion does not generate counter-clockwise but clockwise small-scale overturns at the lower interface. It is unclear how this affects the entrainment of fluid into the

turbulent core. Also, the upward expansion of the upper interface is not hampered by the sea surface here. This interface is therefore much more pronounced than for a near-surface internal hydraulic jump and includes numerous small-scale overturns like at the lower interface. Future modelling may resolve these processes.

Acknowledgments

I thank captain and the crew of the R/V Pelagia for their kind assistance during the sea operations and M. Laan for his enthusiastic development of NIOZ-temperature sensors. The construction of these sensors has been financed in part by NWO. G. Duineveld produced Figure 2. Data requests can be directed to hans.van.haren@nioz.nl.

Disclosure statement

No potential conflict of interest was reported by the authors.

References

Abarbanel, H. D. I., Holm, D. D., Marsden, J. E. and Ratiu, T. 1984. Richardson number criterion for the nonlinear stability of three-dimensional stratified flow. *Phys. Rev. Lett.* **52**, 2352–2355. doi:10.1103/PhysRevLett.52.2352

Armi, L. and Farmer, D. 2002. Stratified flow over topography: bifurcation fronts and transition to the uncontrolled state. *Proc. R Soc. Lond. A* **458**, 513–538. doi:10.1098/rspa.2001.0887

Bogucki, D., Dickey, T., and Redekopp, L. G. 1997. Sediment resuspension and mixing by resonantly generated internal solitary waves. *J. Phys. Oceanogr.* **27**, 1181–1196. doi:10.1175/1520-0485(1997)027<1181:SRAMBR>2.0.CO;2

Cimatoribus, A. A. and van Haren, H. 2015. Temperature statistics above a deep-ocean sloping boundary. *J. Fluid Mech.* **775**, 415–435. doi:10.1017/jfm.2015.295

Cummins, P. F., Armi, L. and Vagle, S. 2006. Upstream internal hydraulic jumps. *J. Phys. Oceanogr.* **36**, 753–769. doi:10.1175/JPO2894.1

Cyr, F., van Haren, H., Mienis, F., Duineveld, G. and Bourgault, D. 2016. On the influence of cold-water coral mound size on flow hydrodynamics, and vice-versa. *Geophys. Res. Lett.* **43**, 775–783. doi:10.1002/2015GL067038

Dale, A. C. and Inall, M. E. 2015. Tidal mixing processes amid small-scale deep-ocean topography. *Geophys. Res. Lett.* **42**, 484–491. doi:10.1002/2014GL062755

Dalziel, S. B., Patterson, M. D., Caulfield, C. P. and Coomaraswamy, A. 2008. Mixing efficiency in high-aspect-ratio Rayleigh–Taylor experiments. *Phys. Fluids* **20**, 065106, 1–14.

Dauxois, T., Didier, A. and Falcon, E. 2004. Observation of near-critical reflection of internal waves in a stably stratified fluid. *Phys. Fluids* **16**, 1936–1941. doi:10.1063/1.1711814

Dillon, T. M. 1982. Vertical overturns: a comparison of Thorpe and Ozmidov length scales. *J. Geophys. Res.* **87**, 9601–9613. doi:10.1029/JC087iC12p09601

Eriksen, C. C. 1982. Observations of internal wave reflection off sloping bottoms. *J. Geophys. Res.* **87**, 525–538. doi:10.1029/JC087iC01p00525

German, C., Klinkhammer, G. P. and Rudnicki, M. 1996. The Rainbow hydrothermal plume, 36 15′ N, MAR. *Geophys. Res. Lett.* **23**, 2979–2982.

Gregg, M. C., D'Asaro, E. A., Riley, J. J. and Kunze, E. 2018. Mixing efficiency in the ocean. *Ann. Rev. Mar. Sci.* **10**, 443–473.

Grue, J., Jensen, A., Rusas, P. O. and Sveen, K. J. 2000. Breaking and broadening of internal solitary waves. *J. Fluid Mech.* **413**, 181–217.

van Haren, H. 2018. Philosophy and application of high-resolution temperature sensors for stratified waters. *Sensors* **18**, 3184.

van Haren, H., Cimatoribus, A. A. and Gostiaux, L. 2015. Where large deep-ocean waves break. *Geophys. Res. Lett.* **42**, 2351–2357.

van Haren, H., Duineveld, G. and de Stigter, H. 2017. Prefrontal bore mixing. *Geophys. Res. Lett.* **44**, 9408–9415.

van Haren, H. and Gostiaux, L. 2012. Detailed internal wave mixing above a deep-ocean slope. *J. Mar. Res.* **70**, 173–197.

van Haren, H., Maas, L. R. M. and Gerkema, T. 2010. Patchiness in internal tidal beams. *J. Mar. Res.* **68**, 237–257.

Hosegood, P., Bonnin, J. and van Haren, H. 2004. Solibore-induced sediment resuspension in the Faeroe-Shetland channel. *Geophys. Res. Lett.* **31**, n/a.

Inall, M. E., Rippeth, T., Griffiths, C. and Wiles, P. 2005. Evolution and distribution of TKE production and dissipation within stratified flow over topography. *Geophys. Res. Lett.* **32**, L08607.

IOC, SCOR, and IAPSO. 2010. The international thermodynamic equation of seawater – 2010: calculation and use of thermodynamic properties. Intergovernmental Oceanographic Commission, Manuals and Guides No. 56, 196pp. Paris, F: UNESCO.

Khripounoff, A., Vangriesheim, A., Crassous, P., Segonzac, M., Colaço, A. and co-authors. 2001. Particle flux in the rainbow hydrothermal vent field (Mid-Atlantic Ridge): dynamics, mineral and biological composition. *J. Mar. Res.* **59**, 633–656.

Klymak, J. M. and Moum, J. N. 2003. Internal solitary waves of elevation advancing on a shoaling shelf. *Geophys. Res. Lett.* **30**.

Legg, S. and Klymak, J. 2008. Internal hydraulic jumps and overturning generated by tidal flow over a tall steep ridge. *J. Phys. Oceanogr.* **38**, 1949–1964.

Miles, J. W. and Howard, L. N. 1964. Note on heterogeneous shear flow. *J. Fluid Mech.* **20**, 331–336.

Mohri, K., Hibiya, T. and Iwamae, N. 2010. Revisiting internal wave generation by tide-topography interaction. *J. Geophys. Res.* **115**, C11001.

Musgrave, R. C., MacKinnon, J. A., Pinkel, R., Waterhouse, A. F. and Nash, J. 2016. Tidally driven processes leading to

near-field turbulence in a channel at the crest of the Mendocino Escarpment. *J. Phys. Oceanogr.* **46**, 1137–1155.

Oakey, N. S. 1982. Determination of the rate of dissipation of turbulent energy from simultaneous temperature and velocity shear microstructure measurements. *J. Phys. Oceanogr.* **12**, 256–271.

Pingree, R. D. and New, A. L. 1991. Abyssal penetration and bottom reflection of internal tidal energy into the Bay of Biscay. *J. Phys. Oceanogr.* **21**, 28–39.

Prandle, D. 1982. The vertical structure of tidal currents. *Geophys. Astrophys. Fluid Dyn.* **22**, 29–49.

Sarkar, S. and Scotti, A. 2017. From topographic internal gravity waves to turbulence. *Annu. Rev. Fluid Mech.* **49**, 195–220.

Slinn, D. N. and Riley, J. J. 1996. Turbulent mixing in the oceanic boundary layer caused by internal wave reflection from sloping terrain. *Dyn. Atmos. Oceans* **24**, 51–62.

Soulsby, R. L. 1983. The bottom boundary layer of shelf seas. In: *Physical Oceanography of Coastal and Shelf Seas* (ed. B. Johns), Amsterdam, NL: Elsevier, pp. 189–266.

Thorpe, S. A. 1977. Turbulence and mixing in a Scottish loch. *Phil. Trans. Roy. Soc. Lond. A* **286**, 125–181.

Thorpe, S. A. 1987. Transitional phenomena and the development of turbulence in stratified fluids: a review. *J. Geophys. Res.* **92**, 5231–5248.

Thorpe, S. A., Malarkey, J., Voet, G., Alford, M. H., Girton, J. B. and co-authors. 2018. Application of a model of internal hydraulic jumps. *J. Fluid Mech.* **834**, 125–148.

Thurnherr, A. M. and Richards, K. J. 2001. Hydrography and high temperature heat flux of the rainbow hydrothermal site (36°14′N, Mid-Atlantic Ridge). *J. Geophys. Res.* **106**, 9411–9426. [CrossRef]

Walter, M., Mertens, C., Stöber, U., German, C. R., Yoerger, D. R. and co-authors. 2010. Rapid dispersal of a hydrothermal plume by turbulent mixing. *Deep-Sea Res. I* **57**, 931–945.

Winters, K. B. 2015. Tidally driven mixing and dissipation in the stratified boundary layer above steep submarine topography. *Geophys. Res. Lett.* **42**, 7123–7130.